Quantification of non-bridging oxygens in silicates using X-ray Raman scattering

E. de Clermont Gallerande, D. Cabaret, G. Radtke, C Sahle, J. M. Ablett, J P Rueff, G. Lelong

Quantification of non-bridging oxygens in silicates using X-ray Raman scattering

E. de Clermont Gallerande[a,*], D. Cabaret[a], G. Radtke[a], C. Sahle[b], J. M. Ablett[c], J.P. Rueff[c], G. Lelong[a,*]

[a] *Sorbonne Université, Muséum National d'Histoire Naturelle, UMR CNRS 7590, IRD, Institut de Minéralogie, de Physique des Matériaux et de Cosmochimie, IMPMC, 75005 Paris, France*
[b] *European Synchrotron Radiation Facility, 38000 Grenoble, France*
[c] *Synchrotron SOLEIL, 91190 Saint-Aubin, France*

Abstract

Detecting and quantifying non-bridging oxygen (NBO) atoms is of particular interest for understanding the physical properties of melts or compressed materials, and requires an unequivocal spectral signature usable during in-situ measurements. In this paper, we evidence a low-energy feature of NBO in lithium silicate crystals using X-ray Raman scattering (XRS) spectroscopy around the energy losses of the oxygen K edge. A specific peak at 534-535 eV in the edge onset is unequivocally attributed to the presence of NBO. Its intensity is used to quantify NBO in lithium silicate glasses. A similar feature at low energy has also been evidenced in Na_2SiO_3 and $MgSiO_3$, generalizing the method to other alkali and alkali-earth silicates. This non-destructive method of NBO quantification, which is based on an X-ray inelastic scattering technique, can be extended to other spectroscopies such as electron-energy loss spectroscopy, soft x-ray absorption spectroscopy at the oxygen K edge.

Keywords: alkali silicates, non-bridging oxygens, XRS, O K edge, vitreous silicates, crystalline silicates

2010 MSC: 00-01, 99-00

*Corresponding author

Email addresses: emmanuelle.de_clermont_gallerande@sorbonne-universite.fr (E. de Clermont Gallerande), gerald.lelong@sorbonne-universite.fr (G. Lelong)

1. Introduction

From Earth's mantle to cutting edge technologies, *silicates* are ubiquitous. Widely spread in industry for ceramics, glass-ceramics, automotive or building applications, they are of primary importance as minerals (olivins, garnets, pyroxenes, serpentines, ...) in the formation and the physical behavior of Earth's interior. All properties of silicates, and more specifically silicate melts, relevant to rock-forming or glass-forming processes, depend on the proportion of non-bridging oxygen (NBO) atoms, *i.e.* oxygen atoms solely bound to a network former cation and bearing a negative charge. The NBO concentration is an indicator of the silica network connectivity and affects material properties, such as viscosity, diffusion, or ionic transport [1, 2, 3, 4, 5, 6, 7, 8].

A full description of the oxygen environment and more specifically the detection and the quantification of NBO atoms appears to be of primary interest in the understanding of melt properties. Electron energy loss spectroscopy (EELS), soft X-ray absorption spectroscopy (XAS) or scanning transmission X-ray microscopy (STXM) can probe the unoccupied states of oxygens [9, 10, 11, 12], and thus bring information on the structure, but no clear spectral signature of NBO atoms in silicates has been reported yet.[13] X-ray photoelectron spectroscopy (XPS) [14, 15, 16], as well as EELS, XAS or STXM, require high-vacuum conditions, which appear to be a limiting factor for carrying out *in situ* high-temperature experiments [17]. Even if ^{17}O triple-quantum magic angle spinning nuclear magnetic resonance (3QMAS NMR) [18, 19, 20, 21] is able to discriminate BO and NBO atoms [22], ^{17}O NMR experiments are still quite challenging under extreme conditions [23, 24, 25, 26, 27, 28].

The determination of the O environment under external constraints thus remains a difficult task because of the technical complexity of probing low-Z elements during *in situ* measurements. Despite such a difficulty, numerous studies have circumvented the problem by calculating a theoretical concentra-

tion of NBO atoms or a number of NBO per SiO_4 tetrahedron (NBO/T) from the chemical composition. This interpolation works well in the case of standard measurements dealing with a silica backbone solely constituted of SiO_4 tetrahedra, but is no more correct as soon as "exotic" coordination numbers of silicon appear in the structure [29]. This can happen when silicate melts are compressed for example. In that case, it is absolutely essential to define new experimental strategies and methods in order to detect and quantify the proportion of NBO atoms.

By probing the K edges of light elements using hard-X-rays [30, 31, 32, 33], allowing to use complex sample environments such as high-pressure cells or high-temperature furnaces, X-ray Raman Scattering (XRS) appears to be an excellent alternative to other spectroscopies [34, 35, 36]. Our recent study on lithium borates has demonstrated the great potentialities of XRS to evidence the presence of NBO atoms using a low energy feature on the O K edge around 535 eV [37, 38]. Is this low-energy feature a universal signature of NBO atoms? Is it possible to monitor it in order to follow the degree of polymerization of a system? To answer to these questions, alkali and alkali-earth silicates have been chosen since they are (i) the base components of numerous Earth's mantle minerals and commercial materials and (ii) prototypic examples of the dimensional reduction of SiO_2 [39, 40].

This paper is focused on probing a spectral signature of NBO atoms in silicates by studying four structures of the Li_2O-SiO_2 binary system as an example of depolymerization processes: SiO_2, $Li_2Si_2O_5$, Li_2SiO_3 and Li_4SiO_4. In order to extend the study to compounds of interest for both materials and Earth Sciences, we also studied the oxygen environment in Na_2SiO_3 and $MgSiO_3$. By coupling calculations based on the Density Functional Theory (DFT) with experimental XRS data, we are able to interpret finely the O K-edge spectra in alkali and alkali-earth silicates and show that the low energy part of the O K edge can be used to probe and quantify NBO atoms.

2. Technical details

2.1. Samples

In order to follow the depolymerization of the silicate network by lithium cations, four crystalline samples from the Li_2O-SiO_2 binary system were prepared with the following molar compositions: quartz-SiO_2, Li_2O:$2SiO_2$, Li_2O:SiO_2, and $2Li_2O$:SiO_2. Two additional crystals, replacing lithium by sodium or magnesium at the metasilicate composition (Na_2O:SiO_2 and MgO:SiO_2) were synthesized for comparison.

The quartz-SiO_2 powder was obtained by crushing a crystal of α-quartz (Herkimer diamond, Herkimer County, New York). For Li_2O:SiO_2, Li_2O:$2SiO_2$ and Na_2O:SiO_2, lithium or sodium carbonate (Li_2CO_3 - 99.99% at Alfa Aesar and Na_2CO_3 - 99.5% at Sigma-Aldrich) and fused silica (reagent grade, 99.5% at Alfa Aesar) were mixed in appropriate quantities and placed in a platinum crucible for melting at 1673 K for Li_2O:SiO_2 and Li_2O:$2SiO_2$ and 1473 K for Na_2O:SiO_2, respectively. Once melted the samples were quenched, ground into powder and heated at 1301 K for 60 h for Li_2O:SiO_2, 773 K for 30 h and 1103 K for 24 h for Li_2O:$2SiO_2$ and 1073 K for 72 h for Na_2O:SiO_2. $2Li_2O$:SiO_2 and MgO:SiO_2 were synthesized using a solid state reaction: Li_2CO_3 (resp. MgO - 98.0% at Merck) and SiO_2 were mixed in appropriate quantities, and heat treated at 1333 K (resp. 1823 K) in a platinum crucible for 6 h interspersed with a grinding every 2 hours.

The purity of the crystalline phases for each compound has been checked using powder X-ray diffraction at the Cu Kα radiation on a Panalytical X'pert pro MPD. Diffractograms were compared with the literature [41, 42, 43, 44, 45, 46], and the following crystalline phases were identified: quartz-SiO_2, $Li_2Si_2O_5$, Li_2SiO_3, Li_4SiO_4, Na_2SiO_3 and $MgSiO_3$. The crystal structures of these six crystals are displayed in Fig. 1 and the crystallographic parameters are summarized in Table 1.

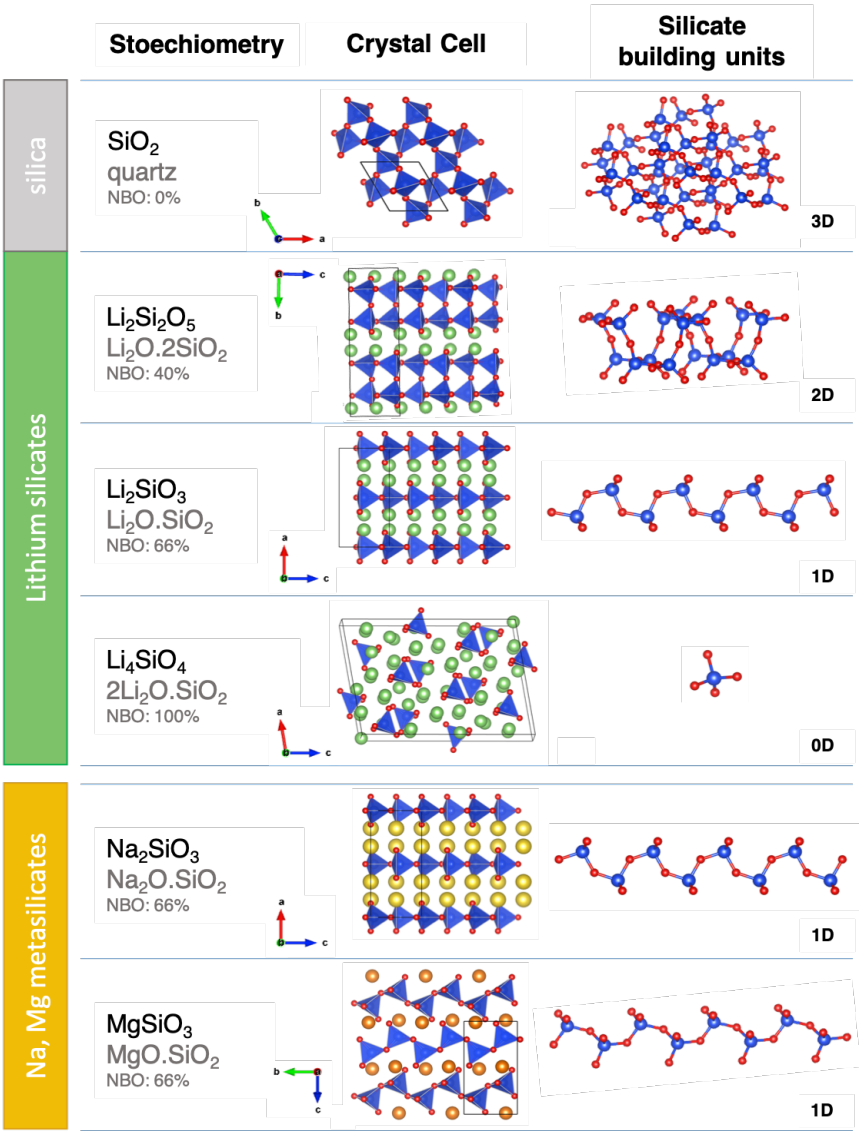

Figure 1: Crystal structure of quartz-SiO_2 [41], $Li_2Si_2O_5$ [42], Li_2SiO_3 [43], Li_4SiO_4 [44], Na_2SiO_3 [45], and $MgSiO_3$ [46]. The structures are also shown through their Si-O framework (Li, Na and Mg atoms are omitted for clarity) and whose dimensions depend on the amount of modifier cation (Li, Na or Mg) in the compounds

Table 1: Structure of SiO_2, $Li_2Si_2O_5$, Li_2SiO_3, Li_4SiO_4, Na_2SiO_3 and $MgSiO_3$.

Crystalline compound	System	Space group	Lattice parameters	O inequivalent sites	Reference
SiO_2	trigonal	$P3_22_1$	$a = 4.921$ Å	1 site	Ref [41]
			$b = 4.921$ Å		
			$c = 5.404$ Å		
			$\gamma = 120°$		
$Li_2Si_2O_5$	monoclinic	Cc	$a = 5.820$ Å	5 sites	Ref [42]
			$b = 14.660$ Å		
			$c = 4.790$ Å		
Li_2SiO_3	orthorhombic	$Cmc2_1$	$a = 9.392$ Å	2 sites	Ref [43]
			$b = 5.397$ Å		
			$c = 4.660$ Å		
Li_4SiO_4	monoclinic	$P2_1/m$	$a = 11.546$ Å	21 sites	Ref [44]
			$b = 6.090$ Å		
			$c = 16.645$ Å		
			$\beta = 99.5°$		
Na_2SiO_3	orthorhombic	$Cmc2_1$	$a = 10.430$ Å	2 sites	Ref [45]
			$b = 6.0200$ Å		
			$c = 4.810$ Å		
$MgSiO_3$	monoclinic	$P2_1/c$	$a = 9.613$ Å	6 sites	Ref [46]
			$b = 8.822$ Å		
			$c = 5.175$ Å		
			$\beta = 108.33°$		

2.2. Experimental details

The XRS measurements were performed at the inelastic scattering beamline ID20 of the European Synchrotron Radiation Facility (ESRF) [47] and at the GALAXIES beamline of synchrotron SOLEIL [48]. Powder samples were placed into 2 mm circular holes drilled in an aluminium sample holder.

For measurements carried out at ID20 beamline (ESRF), we used radiation from 4 U26 undulators that were monochromatized by a high-heat-load Si(111) double crystal monochromator and a successive Si(311) channel-cut monochromator. The monochromatic X-ray beam was focused to approximately $10 \times 20\ \mu m^2$ (V × H) using a Kirkpatrick-Baez mirror. We used the large solid angle spectrometer of ID20 [47] of the ESRF to record the XRS signals. Spectra were collected at a scattering angle 30° for a total of 12 spherically bent Si(660) analyzer crystals. The momentum transfer q was $2.6\,\text{Å}^{-1}$. In order to create losses in the vicinity of the oxygen K edge, we scanned the incident energy from 10.22 to 10.26 keV at a constant analyzer energy of 9.7 keV. The overall energy resolution was 0.7 eV. All data were processed using the XRStools software package [49].

Crystalline lithium silicates were also measured at GALAXIES beamline (synchrotron SOLEIL) in order to check the reproductibility of our measurements and conclusions without any resolution and spectrometer dependance. Datas from ID20 and GALAXIES beamlines are thus treated the same way with an exponential background subtracted to the overall spectra. The curves were smoothed and the spectral integrated intensities were normalized to unity between 530 and 547 eV. A very good agreement can be found between the experimental spectra measured at the two beamlines, so only data from ID20 beamline will be presented in this paper to allowed direct comparison between the diverse compounds.

2.3. Computational details

All the XRS theoretical spectra were performed using XSpectra [50, 51], a module of the suite of codes Quantum Espresso [52]. As Quantum Espresso is based on DFT, uses plane-wave basis set, pseudopotentials and periodic boundary conditions, that implies the use of supercell to avoid interactions between the absorbing atoms and its images. All the *Ultrasoft* pseudopotentials [53]

have been generated using PSLIBRARY [54] in the Rappe, Rabe, Kaxiras, and Joannopoulos formalism [55], within the generalized-gradient approximation of Perdew, Burke and Ernzerhof [56]. The pseudopotential of the oxygen-absorbing atom was obtained by removing one $1s$ electron from its electronic configurations. The Self-Consistent Field (SCF) calculations were carried out using the parameters given in table 2, with an an energy cut-off for electronic wavefunctions of 100 Ry and an energy cut-off for density of 800 Ry. The Full Core-Hole approach (FCH) was used to take the interaction between the electron and the core-hole into account [38].

The XRS spectra were calculated using a $4 \times 4 \times 4$ k-point grid by following the method that we developed in Ref [38]. Each monopole and dipole transitions are calculated as a continued fraction convoluted with an energy-dependent broadening parameter $\gamma(E)$ [57]:

$$\gamma(E) = \Gamma_{\mathrm{H}} + \frac{\Gamma_{\mathrm{M}}}{2} + \frac{\Gamma_{\mathrm{M}}}{\pi} \arctan\left[\frac{\pi}{3}\frac{\Gamma_{\mathrm{M}}}{A_{\mathrm{w}}}\left(x - \frac{1}{x^2}\right)\right], \qquad (1)$$

where $x = (E - E_F)/A_c$, E_F being the Fermi energy, and Γ_{H} the core-hole finite lifetime broadening. The following set of values has been used: $\Gamma_{\mathrm{H}} = 0.2$ eV, $\Gamma_{\mathrm{M}} = 5$ eV, $A_{\mathrm{c}} = 30$ eV and $A_{\mathrm{w}} = 30$ eV. The total O K-edge XRS spectra were convoluted by a Gaussian function to account for the instrumental resolution. When inequivalent crystallographic oxygen sites are present in the structure, each individual calculated spectrum has to be shifted in energy using the ΔSCF approach [37, 38]. Once repositioned, the total spectrum is obtained by calculating a weigthed average of the individual oxygen spectra. A constant energy shift of 535 eV was applied to all the calculated spectra to match with the experimental data. The integrated intensity of the calculated spectra was normalized to unity over the same energy range as the experimental spectra.

Table 2: Calculations parameters for quartz-SiO_2, $Li_2Si_2O_5$, Li_2SiO_3, Li_4SiO_4, Na_2SiO_3, and $MgSiO_3$.

Compound	Supercell	Shortest distance between excited atoms	k-point grid for SCF calculations
SiO_2	$2 \times 2 \times 2$ (72 atoms)	9.842 Å	$3 \times 3 \times 3$
$Li_2Si_2O_5$	$2 \times 1 \times 2$ (144 atoms)	9.580 Å	$2 \times 2 \times 2$
Li_2SiO_3	$1 \times 2 \times 2$ (96 atoms)	9.320 Å	$3 \times 3 \times 3$
Li_4SiO_4	$1 \times 2 \times 1$ (252 atoms)	11.546 Å	$1 \times 1 \times 1$
Na_2SiO_3	$1 \times 2 \times 3$ (144 atoms)	10.430 Å	$2 \times 2 \times 2$
$MgSiO_3$	$1 \times 1 \times 2$ (80 atoms)	8.822 Å	$3 \times 3 \times 3$

3. Results and discussion

3.1. Evidence of a spectral signature of non-bridging oxygens

The Li_2O-SiO_2 binary is an archetypical example of dimensional reduction of a framework constituted by corner-sharing tetrahedra (Fig. 1) [40]. When Li_2O is incorporated into quartz-SiO_2, the tridimensional structure of quartz (SiO_2) is gradually transformed into layers ($Li_2Si_2O_5$), infinite chains (Li_2SiO_3), dimers ($Li_6Si_2O_7$) and monomers (Li_4SiO_4) [39] (Fig. 1). Except for SiO_2, all the crystallographic structures present a partially or a fully depolymerized silicate network characterized by the presence of NBOs. While quartz-SiO_2 is used as a reference of a fully polymerized network solely composed of bridging oxygens, $Li_2Si_2O_5$, Li_2SiO_3 and Li_4SiO_4 contain one, two and four NBO atoms per SiO_4 tetrahedron, respectively. Unambigously, addition of lithium ions leads to drastic changes in the O K-edge XRS spectra (Fig. 2). The O K-edge spectrum of quartz-SiO_2 is characterized by an intense peak around 538-539 eV corresponding to electronic transition from a $1s$ core state to unoccupied antibonding σ^* orbitals of the SiO_4 tetrahedral units [58]. With the addition of alkali cations into SiO_2, the intensity of this feature decreases from SiO_2 to Li_4SiO_4 and an additional peak rises at $\sim$ 534-535 eV, whose intensity increases with the alkali content and the presence of NBOs.

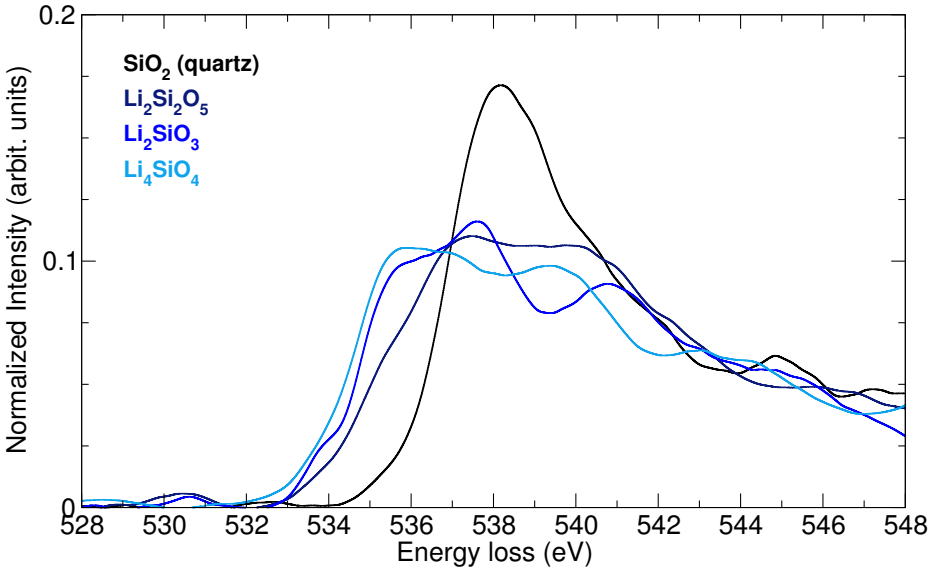

Figure 2: Experimental O K-edge XRS spectra of quartz-SiO_2 (black), $Li_2Si_2O_5$ (dark blue), Li_2SiO_3 (blue) and Li_4SiO_4 (light blue) measured at $q = 2.6\,\text{Å}^{-1}$. The low-energy feature around 534-535 eV is a signature of the non-bridging oxygen atoms in silicates.

The calculated O K-edge XRS spectra are compared to the experimental data in Fig. 3. Simulations reproduce well the overall shape of the experimental spectra with slightly more contracted features which is known to be related to the use of DFT [50, 60], in particular to neglect of self-energy effects [59]. Since calculations take all the inequivalent oxygen atoms into account, it is possible to decipher the contributions from BO and NBO atoms. From the calculated decomposition, the low-energy feature at $\sim$ 534-535 eV can be attributed to electronic transitions from the $1s$ core state to the σ^* states of oxygen in SiO_4 units solely related to NBO atoms. The peak attributed to BO atoms is shifted of about 1.5 eV to appear at $\sim$ 536 eV. This core-level shift, also observed in lithium borates, can be explained by a difference in the screening efficiency of the core-hole by the valence electron density between BO and NBO atoms [37].

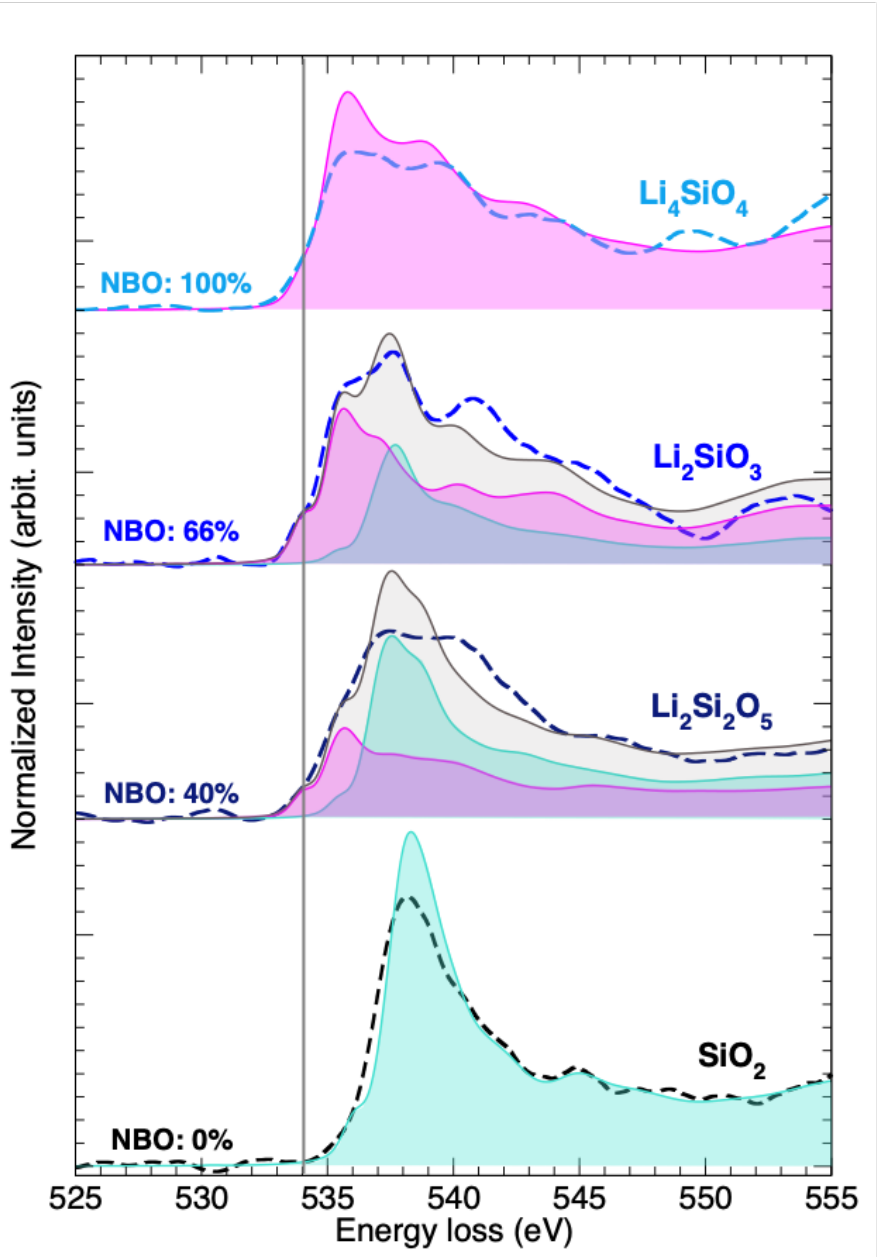

Figure 3: Comparison between experimental (dashed) and theoretical (solid) XRS O K-edge spectra of quartz-SiO_2, $Li_2Si_2O_5$, Li_2SiO_3 and Li_4SiO_4 at $q = 2.6\,\text{Å}$. The contribution of NBO is in magenta, and the contribution of BO is in cyan.

The O K-edge spectrum of lithium silicates is very sensitive to the presence of NBO atoms in the first few eVs of the absorption edge. The spectral signature at $\sim$ 534-535 eV in silicates can be used as a direct proxy of NBO atoms, whose a quantification would be of primary interest. The calculated XRS spectra show that fitting the pre-edge of the O K-edge spectrum with Gaussian functions may not be reliable. For example, in the case of $Li_2Si_2O_5$ (Fig. 3), BO and NBO contributions overlap from 535 eV which does not allow to separate both contributions reliably. The intensity at 534 eV, which is free from any BO contribution, is a good indicator of the proportion of NBO in the sample. A linear relation is indeed found between the normalized intensity at 534 eV and the known proportion of NBO atoms present in each crystalline phase (Fig. 4(a)). This trend is also supported by the DFT calculations, which show an excellent agreement with the experimental values (Fig. 4(b)). This proportionality means that the NBO content can be straitforwardly estimated using the following equation:

$$\%NBO = 2335 \times I(534 \text{ eV}) \tag{2}$$

where $I(534 \text{ eV})$ is the intensity measured at 534 eV.

This relation is valid on a 0-66% range of NBO concentration, above which a deviation is observed. Similarly to the case of lithium borates [37], the NBO peak of the orthosilicate composition slightly shifts towards higher energies. As a consequence, the intensity at 534 eV is underestimated in the critical case of an isolated SiO_4^{4-} anion. For NBO concentration up to 66%, Eq. 2 can be used to quantify the ratio of NBO atoms in materials in which the concentration is unknown, such as in amorphous materials, liquids or high-pressure compounds.

In order to test the reliability of Eq. 2, three lithium silicate glasses (v-SiO_2, v-$Li_2Si_2O_5$ and v-Li_2SiO_3) were measured in the same experimental conditions (Fig. 5(a)). The experimental intensities measured at 534 eV on the O K-edge XRS spectra give values equal to 0.001, 0.021 and 0.027, corresponding to 3%,

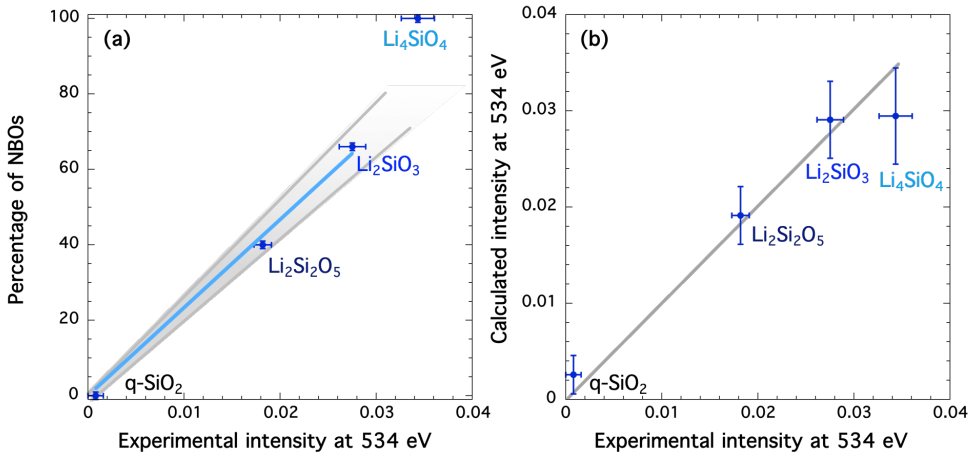

Figure 4: (a) Percentage of NBO as a function of the experimental intensity measured at 534 eV in the O K edge of four crystalline structures of the Li_2O-SiO_2 binary: quartz-SiO_2, $Li_2Si_2O_5$, Li_2SiO_3 and Li_4SiO_4. The blue line represent a linear least-squares fit of the first three crystals and the grey shaded area is indicative of the validity domain. (b) Correlation of the experimental intensity at 534 eV with the calculated intensity at 534 eV. The grey line is a guide for the eyes for a full correlation.

49% and 64% of NBOs in v-SiO_2, v-$Li_2Si_2O_5$ and v-Li_2SiO_3, respectively. The uncertainties on these values based on the signal-to-noise ratio and background subtraction is estimated to $\pm$ 5%. To keep charge neutrality, each lithium cation (Li^+) has to be charge balanced by a single NBO, leading to theoretical NBO ratios of 0%, 40% and 66% for v-SiO_2, v-$Li_2Si_2O_5$ and v-Li_2SiO_3, respectively (Fig. 5(b)). An excellent agreement is found with the present XRS results, but also with the values deduced from ^{29}Si MAS-NMR from which an estimate of NBO's proportion via the distribution of Q^n groups can be deduced [61, 62, 63, 64, 65]. The proposed equation appears to be a reliables method for the determination and the quantification of NBOs in the Li_2O-SiO_2 system.

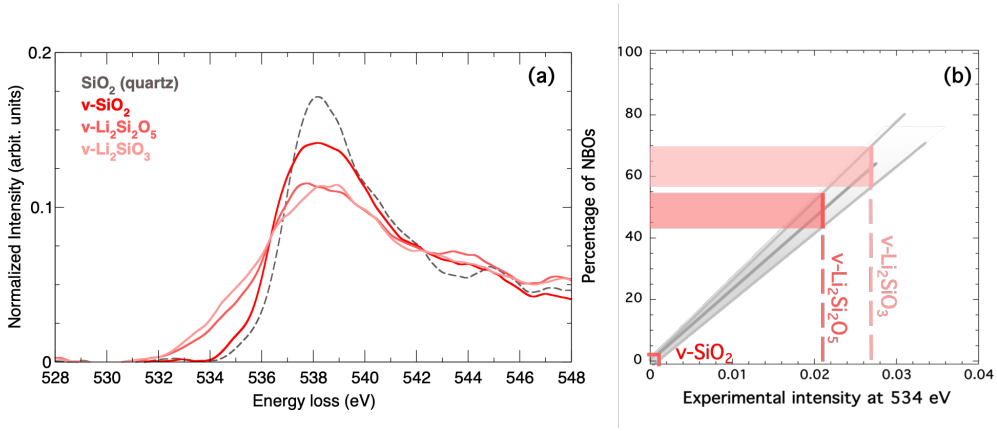

Figure 5: (a) O K-edge XRS spectra of three glassy samples of the Li_2O-SiO_2 binary: v-SiO_2, v-$Li_2Si_2O_5$ and v- Li_2SiO_3. The α-quartz SiO_2 (black dashed line) is shown as a reference sample fully constituted by BO. (b) Quantification of the proportion of NBOs in these three glasses using the equation defined in Fig. 4(a)

3.2. Influence of the modifier cation on the NBO spectral signature

The spectral feature of NBO atoms in lithium silicates is clearly evidenced, and the NBO quantification is accessible using an X-ray inelastic scattering based technique. It is now relevant to try generalizing this approach to others silicates such as sodium and magnesium silicates, which are of particular relevance for both material and Earth science communities.

The O K-edge XRS spectra of Li_2SiO_3, Na_2SiO_3 and $MgSiO_3$ are shown in Figure 6 accompanied with the one of quartz-SiO_2, a fully polymerized reference compound. Unequivocally, the sodium and magnesium metasilicates show the same spectral signature of NBOs than the lithium metasilicate, *i.e.* an additional peak arising at low-energy in the O K-edge spectrum [9], the small peak at 530.5 eV is due to beam damages [9, 66]. The main difference resides in the position of the edge jump, *i.e.*, 532.2 eV for Na_2O, 532.7 eV for Li_2O and 533.2 eV for MgO. Since these three compounds have very similar medium-range order (Fig. 1), the origin of this shift has to be related to a more local property such as the polarizing power of the modifier network cation, which is

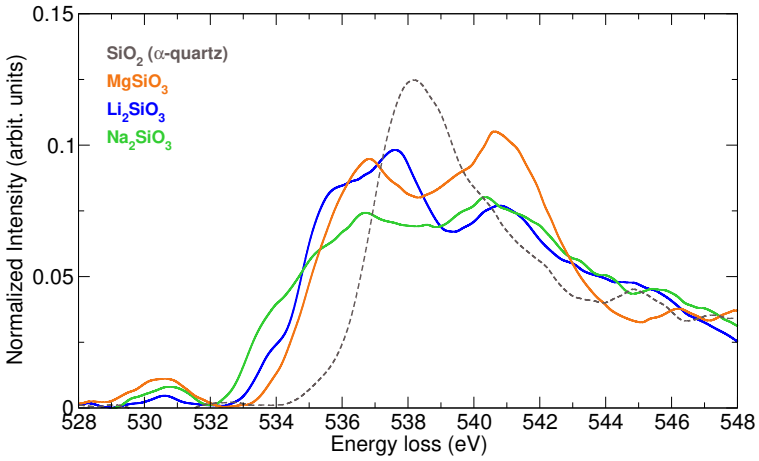

Figure 6: O K-edge spectra of of Li_2SiO_3 (blue), Na_2SiO_3 (green) and $MgSiO_3$ (orange). The α-quartz SiO_2 (black dashed line) is shown as a reference sample fully constituted by BO.

directly related to their field strength: Na^+ ($F_S = 0.19\,\text{Å}^2$), Li^+ ($F_S = 0.23\,\text{Å}^2$) and Mg^{2+} ($F_S = 0.45\,\text{Å}^2$) [67, 68]. The addition of a modifier oxide may lead to a change in the electronic structure of the silicate units, as the presence of modifier cation tends to increase the ionic character of the Si-O network [69, 70]. The delocalization of the electronic density around oxygen atoms would be more important in the case of Na^+ in comparison with Li^+ and Mg^+, which gives a more ionic character to the Na-O bond than to the Li-O or Mg-O bond. As a consequence, the difference of polarization between NBO and BO would increase with the cation field strength, leading to an increase of the chemical shift (ΔE) between the two contributions of about 1 eV between Na and Li and of about 0.5 eV between Li and Mg. A similar variation of ΔE between Na- and Li-silicate glasses was deduced from XPS O $1s$ measurements, corroborating the present results [69, 16]. More interestingly, these XPS measurements give evidence that an even higher chemical shift between BO and NBO atoms will be found for potassium and caesium silicates.

In the low q configuration employed here, solely the dipole component con-

tributes significantly to the total spectrum. Since XAS ans EELS are mainly governed by dipole transitions, this spectral feature at low energy in the O K edge becomes a universal signature of NBOs for X-ray and electron based spectroscopies. The quantification of NBOs in silicates is achievable by determining a dedicated relation for each alkali oxide or alkaline-earth oxide / SiO_2 binary. This non-destructive method of quantification of NBOs, which is based on an X-ray inelastic scattering technique, will allow in a close future an *in-situ* monitoring of NBOs in materials placed under external constraints.

4. Conclusion

The O K-edge XRS measurements of the four crystalline compounds of the Li_2O-SiO_2 system and the theoretical calculations show the presence of an additional feature at low-energy around 534-535 eV that can be unambiguously associated with the presence of non-bridging oxygen atoms. The intensity of this feature is proportional to the NBO content for fully and partially depolymerized compounds. By using crystalline references, an equation between the intensity at 534 eV and the NBO content has been established and used to determine the amount of NBO on vitreous lithium silicates. A similar feature at low energy has also been evidenced in Na_2SiO_3 and $MgSiO_3$, generalizing the method to other alkali and alkali-earth silicates. The determination and the quantification of NBOs developed here using XRS is also transferrable to similar spectroscopic techniques, such as EELS, soft-XAS and STXM. As XRS allows *in situ* measurements, it opens the way to novel investigations on silicate compounds placed in complex sample environments such as high-pressure or high-temperature cells.

5. Acknowledgement

This work was granted access to the HPC resources of IDRIS under the allocation A0020906863 made by GENCI (Grand Equipement National de Calcul Intensif). This work was supported by French state funds managed by the ANR

within the Investissements d'Avenir programme under reference ANR-11-IDEX-0004-02, and more specifically within the framework of the Cluster of Excellence MATISSE led by Sorbonne Universités. We acknowledge the ESRF and Synchrotron SOLEIL for providing synchrotron radiation and technical support.

References

[1] M. Hayashi, H. Ishii, M. Susa, H. Fukuyama, K. Nagata, Effect of ionicity of nonbridging oxygen ions on thermal conductivity of molten alkali silicates, Phys. Chem. Glasses 42 (1) (2001) 6–11.

[2] K. Otto, M. E. Milberg, Ionic Conduction in Alkali and Thallium Silicate Glasses, J. Am. Ceram. Soc. 51 (6) (1968) 326–329. doi:http://dx.doi.org/10.1111/j.1151-2916.1968.tb15947.x.

[3] T. Ohkubo, E. Tsuchida, M. Gobet, V. Sarou-Kanian, C. Bessada, Y. Iwadate, First-Principles Molecular Dynamics Simulation and Conductivity Measurements of a Molten xLi_2O-(1-x)B_2O_3 System, J. Phys. Chem. B 117 (18) (2013) 5668–5674. doi:http://dx.doi.org/10.1021/jp312486m.

[4] B. O. Mysen, Structure and properties of silicate melts, Elsevier Science & Technology Books, 1988.

[5] O. V. Mazurin, Handbook of glass data, Elsevier, 1983.

[6] R. J. Charles, The Mixed Alkali Effect in Glasses, J. Am. Ceram. Soc. 48 (8) (1965) 432–434.

[7] D. R. Neuville, P. Richet, Viscosity and mixing in molten (Ca, Mg) pyroxenes and garnets, Geochim. Cosmochim. Acta 55 (4) (1991) 1011–1019. doi:http://dx.doi.org/10.1016/0016-7037(91)90159-3.

[8] B. O. Mysen, D. Virgo, A. S. Friedrich, The Structure of Silicate Melts: Implications for Chemical and Physical Properties of Natural Magma, Rev. Geophys. 20 (3) (1982) 353–383.

[9] L. A. J. Garvie, Can electron energy-loss spectroscopy (EELS) be used to quantify hydrogen in minerals from the O K edge?, Am. Min. 95 (1) (2010) 92–97. doi:http://dx.doi.org/10.2138/am.2010.3290.

[10] G. S. Henderson, D. R. Neuville, L. Cormier, An O K-edge XANES study of calcium aluminates, Can. J. Chem. 85 (10) (2007) 801–805. doi:http://dx.doi.org/10.1139/v07-071.

[11] D. Cabaret, F. Mauri, G. S. Henderson, Oxygen K-edge XANES of germanates investigated using first-principles calculations, Phys. Rev. B 75 (18) (2007) 184205. doi:http://dx.doi.org/10.1103/PhysRevB.75.184205.

[12] H. J. Nilsson, T. Tyliszczak, R. E. Wilson, L. Werme, D. K. Shuh, Soft X-ray scanning transmission X-ray microscopy (STXM) of actinide particles, Anal. Bioanal. Chem. 383 (1) (2005) 41–47. doi:http://dx.doi.org/10.1007/s00216-005-3355-5.

[13] N. Jiang, On detection of non-bridging oxygen in glasses by electron-energy-loss spectroscopy, Solid State Commun. 122 (1-2) (2002) 7–10. doi:http://dx.doi.org/10.1016/S0038-1098(02)00092-3.

[14] H. W. Nesbitt, G. M. Bancroft, G. S. Henderson, R. Ho, K. N. Dalby, Y. Huang, Z. Yan, Bridging, non-bridging and free (O^{2-}) oxygen in Na_2O-SiO_2 glasses: An X-ray Photoelectron Spectroscopic (XPS) and Nuclear Magnetic Resonance (NMR) study, J. Non Cryst. Solids 357 (1) (2011) 170–180. doi:http://dx.doi.org/10.1016/j.jnoncrysol.2010.09.031.

[15] W. Y. Ching, Y. P. Li, B. W. Veal, D. J. Lam, Electronic structures of lithium metasilicate and lithium disilicate, Phys. Rev. B 32 (2) (1985) 1203–1207. doi:http://dx.doi.org/10.1103/PhysRevB.32.1203.

[16] R. Brückner, H.-U. Chun, H. Goretzki, M. Sammet, XPS measurements and structural aspects of silicate and phosphate glasses, J. Non Cryst. Solids

42 (1-3) (1980) 49–60. doi:http://dx.doi.org/10.1016/0022-3093(80)90007-1.

[17] H. W. Nesbitt, G. M. Bancroft, High Resolution Core- and Valence-Level XPS Studies of the Properties (Structural, Chemical and Bonding) of Silicate Minerals and Glasses, Rev. Mineral. Geochem. 78 (1) (2014) 271–329. doi:http://dx.doi.org/10.2138/rmg.2014.78.7.

[18] T. Charpentier, S. Ispas, M. Profeta, F. Mauri, C. J. Pickard, First-Principles Calculation of ^{17}O, ^{29}Si, and ^{23}Na NMR Spectra of Sodium Silicate Crystals and Glasses, J. Phys. Chem. B 108 (13) (2004) 4147–4161. doi:http://dx.doi.org/10.1021/jp0367225.

[19] J. F. Stebbins, J. V. Oglesby, S. K. Lee, Oxygen sites in silicate glasses: a new view from oxygen-17 NMR, Chemical Geology 174 (1-3) (2001) 63–75. doi:http://dx.doi.org/10.1016/S0009-2541(00)00307-7.

[20] I. Farnan, P. J. Grandinetti, J. H. Baltisberger, J. F. Stebbins, U. Werner, M. A. Eastman, A. Pines, Quantification of the disorder in network-modified silicate glasses, Nature 358 (6381) (1992) 31. doi:http://dx.doi.org/10.1038/358031a0.

[21] J. F. Stebbins, J. Wu, L. M. Thompson, Interactions between network cation coordination and non-bridging oxygen abundance in oxide glasses and melts: Insights from NMR spectroscopy, Chemical Geology 346 (2013) 34–46. doi:http://dx.doi.org/10.1016/j.chemgeo.2012.09.021.

[22] S. Lee, K. Mibe, Y. Fei, G. D. Cody, B. O. Mysen, Structure of B 2 O 3 Glass at High Pressure: A B 11 Solid-State NMR Study, Phys. Rev. Lett. 94 (16). doi:http://dx.doi.org/10.1103/PhysRevLett.94.165507.

[23] T. Meier, S. Khandarkhaeva, S. Petitgirard, T. Körber, A. Lauerer, E. Rssler, L. Dubrovinsky, NMR at pressures up to 90 GPa, J. Magn. Reson. 292 (2018) 44–47. doi:http://dx.doi.org/10.1016/j.jmr.2018.05.002.

[24] M. G. Pravica, I. F. Silvera, Nuclear magnetic resonance in a diamond anvil cell at very high pressures, Review of Scientific Instruments 69 (2) (1998) 479–484. doi:http://dx.doi.org/10.1063/1.1148686.

[25] A. M. George, P. Richet, J. F. Stebbins, Cation dynamics and premelting in lithium metasilicate (Li_2SiO_3) and sodium metasilicate (Na_2SiO_3): A high-temperature NMR study, Am. Min. 83 (1998) 1277–1284.

[26] D. Massiot, F. Fayon, V. Montouillout, N. Pellerin, J. Hiet, C. Roiland, P. Florian, J.-P. Coutures, L. Cormier, D. R. Neuville, Structure and dynamics of oxide melts and glasses: A view from multinuclear and high temperature NMR, J. Non Cryst. Solids 354 (2-9) (2008) 249–254. doi:http://dx.doi.org/10.1103/PhysRevLett.94.16550710.1016/j.jnoncrysol.2007.06.097.

[27] J. F. Stebbins, Chapter 9 : NMR at High Temperature, in: Modern Methods in Solid-state NMR, Royal Society of Chemistry, 2018, pp. 262–288. doi:http://dx.doi.org/10.1039/9781788010467-00262.

[28] J. F. Stebbins, I. Farnan, X. Xue, The structure and dynamics of alkali silicate liquids: A view from NMR spectroscopy, Chemical Geology 96 (3) (1992) 371–385. doi:http://dx.doi.org/10.1016/0009-2541(92)90066-E.

[29] S. Petitgirard, C. J. Sahle, C. Weis, K. Gilmore, G. Spiekermann, J. S. Tse, M. Wilke, C. Cavallari, V. Cerantola, C. Sternemann, Magma properties at deep Earth's conditions from electronic structure of silica, Geochem. Perspect. Lett. (2019) 32–37doi:http://dx.doi.org/10.7185/geochemlet.1902.

[30] G. Lelong, L. Cormier, L. Hennet, F. Michel, J.-P. Rueff, J. M. Ablett, G. Monaco, Lithium borate crystals and glasses: How similar are they? A non-resonant inelastic X-ray scattering study around the B and O K -edges, J. Non Cryst. Solids 472 (2017) 1–8. doi:http://dx.doi.org/10.1016/j.jnoncrysol.2017.06.012.

[31] U. Bergmann, P. Glatzel, S. P. Cramer, Bulk-sensitive XAS characterization of light elements: from X-ray Raman scattering to X-ray Raman spectroscopy, Microchem. J. 71 (2-3) (2002) 221–230. doi:http://dx.doi.org/10.1016/S0026-265X(02)00014-0.

[32] C. Sternemann, M. Wilke, Spectroscopy of low and intermediate Z elements at extreme conditions: in situ studies of Earth materials at pressure and temperature via X-ray Raman scattering, High Pressure Research 36 (3) (2016) 275–292. doi:http://dx.doi.org/10.1080/08957959.2016.1198903.

[33] P. Wernet, D. Nordlund, U. Bergmann, M. Cavalleri, M. Odelius, H. Ogasawara, L. A. Nslund, T. K. Hirsch, L. Ojamäe, P. Glatzel, L. G. M. Pettersson, A. Nilsson, The Structure of the First Coordination Shell in Liquid Water, Science 304 (5673) (2004) 995–999. doi:http://dx.doi.org/10.1126/science.1096205.

[34] S. K. Lee, P. J. Eng, H.-K. Mao, J. Shu, Probing and modeling of pressure-induced coordination transformation in borate glasses: Inelastic x-ray scattering study at high pressure, Phys. Rev. B 78 (21). doi:http://dx.doi.org/10.1103/PhysRevB.78.214203.

[35] S. K. Lee, P. J. Eng, H.-K. Mao, Y. Meng, J. Shu, Structure of Alkali Borate Glasses at High Pressure: B and Li K -Edge Inelastic X-Ray Scattering Study, Phys. Rev. Lett. 98 (10). doi:http://dx.doi.org/10.1103/PhysRevLett.98.105502.

[36] G. Lelong, L. Cormier, G. Ferlat, V. Giordano, G. S. Henderson, A. Shukla, G. Calas, Evidence of fivefold-coordinated Ge atoms in amorphous GeO_2 under pressure using inelastic x-ray scattering, Phys. Rev. B 85 (13). doi:http://dx.doi.org/10.1103/PhysRevB.85.134202.

[37] G. Lelong, G. Radtke, L. Cormier, H. Bricha, J.-P. Rueff, J. M. Ablett, D. Cabaret, F. Gélébart, A. Shukla, Detecting Non-bridging Oxygens: Non-Resonant Inelastic X-ray Scattering in Crystalline Lithium Borates, Inorg.

Chem. 53 (20) (2014) 10903–10908. doi:http://dx.doi.org/10.1021/ic501730q.

[38] E. de Clermont Gallerande, D. Cabaret, G. Lelong, C. Brouder, M.-B. Attaiaa, L. Paulatto, K. Gilmore, C. J. Sahle, G. Radtke, First-principles modeling of x-ray Raman scattering spectra, Phys. Rev. B 98 (21). doi:http://dx.doi.org/10.1103/PhysRevB.98.214104.

[39] G. Rousse, B. Baptiste, G. Lelong, Crystal Structures of $Li_6B_4O_9$ and $Li_3B_{11}O_{18}$ and Application of the Dimensional Reduction Formalism to Lithium Borates, Inorg. Chem. 53 (12) (2014) 6034–6041. doi:http://dx.doi.org/10.1021/ic500331u.

[40] E. G. Tulsky, J. R. Long, Dimensional Reduction: A Practical Formalism for Manipulating Solid Structures, Chemistry of Materials 13 (4) (2001) 1149–1166. doi:http://dx.doi.org/10.1021/cm0007858.

[41] H. d'Amour, W. Denner, H. Schulz, Structure determination of α-quartz up to 68 x 10^8 Pa, Acta Crystallogr. B 35 (3) (1979) 550–555. doi:http://dx.doi.org/10.1107/S056774087900412X.

[42] F. Liebau, Untersuchungen an Schichtsilikaten des Formeltyps $Am(Si_2O_5)n$. I. Die Kristallstruktur der Zimmertemperaturform des $Li_2Si_2O_5$., Acta Crystallogr. 14 (4) (1961) 389–395. doi:http://dx.doi.org/10.1107/S0365110X61001303.

[43] K. F. Hesse, Refinement of the crystal structure of lithium polysilicate, Acta Crystallogr. B 33 (3) (1977) 901–902. doi:http://dx.doi.org/10.1107/S0567740877004932.

[44] D. Tranqui, R. D. Shannon, H.-Y. Chen, S. Iijima, W. H. Baur, Crystal structure of ordered Li_4SiO_4, Acta Crystallogr. B 35 (11) (1979) 2479–2487. doi:http://dx.doi.org/10.1107/S0567740879009730.

[45] A. Grund, M. Pizy, Structure cristalline du metasilicate de sodium anhydre, Na_2SiO_3, Acta Crystallogr. 5 (6) (1952) 837–840. doi:http://dx.doi.org/10.1107/S0365110X52002239.

[46] M. Kanzaki, X. Xue, Protoenstatite in $MgSiO_3$ samples prepared by conventional solid state reaction, J. M. P. S. 112 (6) (2017) 359–364. doi:http://dx.doi.org/10.2465/jmps.170616.

[47] S. Huotari, C. J. Sahle, C. Henriquet, A. Al-Zein, K. Martel, L. Simonelli, R. Verbeni, H. Gonzalez, M.-C. Lagier, C. Ponchut, M. Moretti Sala, M. Krisch, G. Monaco, A large-solid-angle X-ray Raman scattering spectrometer at ID20 of the European Synchrotron Radiation Facility, J. Synchrotron Radiat. 24 (2) (2017) 521–530. doi:http://dx.doi.org/10.1107/S1600577516020579.

[48] J. M. Ablett, D. Prieur, D. Céolin, B. Lassalle-Kaiser, B. Lebert, M. Sauvage, T. Moreno, S. Bac, V. Balédent, A. Ovono, M. Morand, F. Gélébart, A. Shukla, J.-P. Rueff, The GALAXIES inelastic hard X-ray scattering end-station at Synchrotron SOLEIL, J. Synchrotron Radiat. 26 (1). doi:http://dx.doi.org/10.1107/S160057751801559X.

[49] C. J. Sahle, A. Mirone, J. Niskanen, J. Inkinen, M. Krisch, S. Huotari, Planning, performing and analyzing X-ray Raman scattering experiments, J. Synchrotron Radiat. 22 (2) (2015) 400–409. doi:http://dx.doi.org/10.1107/S1600577514027581.

[50] M. Taillefumier, D. Cabaret, A.-M. Flank, F. Mauri, X-ray absorption near-edge structure calculations with the pseudopotentials: Application to the K-edge in diamond and α-quartz, Phys. Rev. B 66 (19). doi:http://dx.doi.org/10.1103/PhysRevB.66.195107.

[51] C. Gougoussis, M. Calandra, A. P. Seitsonen, F. Mauri, First-principles calculations of x-ray absorption in a scheme based on ultrasoft pseudopotentials: From α-quartz to high- T_c compounds, Phys. Rev. B 80 (7). doi:http://dx.doi.org/10.1103/PhysRevB.80.075102.

[52] P. Giannozzi, S. Baroni, N. Bonini, M. Calandra, R. Car, C. Cavazzoni, D. Ceresoli, G. L. Chiarotti, M. Cococcioni, I. Dabo, A. Dal Corso, S. de Gironcoli, S. Fabris, G. Fratesi, R. Gebauer, U. Gerstmann, C. Gougoussis, A. Kokalj, M. Lazzeri, L. Martin-Samos, N. Marzari, F. Mauri, R. Mazzarello, S. Paolini, A. Pasquarello, L. Paulatto, C. Sbraccia, S. Scandolo, G. Sclauzero, A. P. Seitsonen, A. Smogunov, P. Umari, R. M. Wentzcovitch, QUANTUM ESPRESSO: a modular and open-source software project for quantum simulations of materials, J. Phys. Condens. Matter 21 (39) (2009) 395502. doi:http://dx.doi.org/10.1088/0953-8984/21/39/395502.

[53] D. Vanderbilt, Soft self-consistent pseudopotentials in a generalized eigenvalue formalism, Phys. Rev. B 41 (11) (1990) 7892–7895. doi:http://dx.doi.org/10.1103/PhysRevB.41.7892.

[54] A. Dal Corso, Pseudopotentials periodic table: From h to pu, Comput. Mat. Sci. 95 (2014) 337–350.

[55] A. M. Rappe, K. M. Rabe, E. Kaxiras, J. D. Joannopoulos, Optimized pseudopotentials, Phys. Rev. B 41 (1990) 1227–12230.

[56] J. P. Perdew, K. Burke, M. Ernzerhof, Generalized gradient approximation made simple, Phys. Rev. Lett. 77 (1996) 3865–3868.

[57] M. P. Seah, W. A. Dench, Quantitative Electron Spectroscopy of Surfaces - a Strandard Data Base for Electron Inelastic Mean Free Paths in Solids, Vol. 82, National Physical Laboratory, Division of Chemical Standards, 1978.

[58] J.-F. Lin, H. Fukui, D. Prendergast, T. Okuchi, Y. Q. Cai, N. Hiraoka, C.-S. Yoo, A. Trave, P. Eng, M. Y. Hu, P. Chow, Electronic bonding transition in compressed SiO2 glass, Phys. Rev. B 75 (1) (2007) 012201. doi:http://dx.doi.org/10.1103/PhysRevB.75.012201.

[59] J. J. Kas, J. Vinson, N. Trcera, D. Cabaret, E. L. Shirley, J. J. Rehr, Many-pole model of inelastic losses applied to calculations of XANES, J. Phys. Conf. Ser. 190 (2009) 012009. doi:http://dx.doi.org/10.1088/1742-6596/190/1/012009.

[60] W. Olovsson, I. Tanaka, P. Puschnig, C. Ambrosch-Draxl, Near-edge structures from first principles all-electron Bethe-Salpeter equation calculations, J. Phys. Condens. Matter 21 (10) (2009) 104205. doi:http://dx.doi.org/10.1088/0953-8984/21/10/104205.

[61] C. Larson, J. Doerr, M. Affatigato, S. Feller, D. Holland, M. E. Smith, A ^{29}Si MAS NMR study of silicate glasses with a high lithium content, J. Phys. Condens. Matter 18 (49) (2006) 11323–11331. doi:http://dx.doi.org/10.1088/0953-8984/18/49/023.

[62] H. Maekawa, T. Maekawa, K. Kawamura, T. Yokokawa, The structural groups of alkali silicate glasses determined from ^{29}Si MAS-NMR, J. Non Cryst. Solids 127 (1) (1991) 53–64. doi:http://dx.doi.org/10.1016/0022-3093(91)90400-Z.

[63] J. Du, L. R. Corrales, Characterization of the Structural and Electronic Properties of Crystalline Lithium Silicates, J. Phys. Chem. B 110 (45) (2006) 22346–22352. doi:http://dx.doi.org/10.1021/jp056879s.

[64] R. Dupree, D. Holland, M. G. Mortuza, A MAS-NMR investigation of lithium silicate glasses and glass ceramics, J. Non Cryst. Solids 116 (2-3) (1990) 148–160. doi:http://dx.doi.org/10.1016/0022-3093(90)90687-H.

[65] U. Voigt, H. Lammert, H. Eckert, A. Heuer, Cation clustering in lithium silicate glasses: Quantitative description by solid-state NMR and molecular dynamics simulations, Phys. Rev. B 72 (6) (2005) 064207. doi:http://dx.doi.org/10.1103/PhysRevB.72.064207.

[66] N. Jiang, J. Qiu, A. Ellison, J. Silcox, Fundamentals of high-energy electron-irradiation-induced modifications of silicate glasses, Phys. Rev. B 68 (6). doi:http://dx.doi.org/10.1103/PhysRevB.68.064207.

[67] A. Dietzel, Die kationenfeldstärken und ihre beziehungen zu entglasungsvorgngen, zur verbindungsbildung und zu den schmelzpunkten von silicaten, Ztschr. Elektrochem. 48 (1) (1942) 9–23. doi:http://dx.doi.org/10.1002/bbpc.19420480104.

[68] A. K. Varshneya, Fundamentals of inorganic glasses, Elsevier, 2013.

[69] R. Brückner, H.-U. Chun, H. Goretzki, XPS-Measurements on Alkali Silicate and Soda Aluminosilicate Glasses, Jpn. J. Appl. Phys. 17 (S2) (1978) 291. doi:http://dx.doi.org/10.7567/JJAPS.17S2.291.

[70] G. Wiech, E. Zöpf, H.-U. Chun, R. Brückner, X-ray spectroscopic investigation of the structure of silica, silicates and oxides in the crystalline and vitreous state, J. Non Cryst. Solids 21 (2) (1976) 251–261. doi:http://dx.doi.org/10.1016/0022-3093(76)90046-6.